Article

Discovery Medicine 2025; 37(195): 669–684
https://doi.org/10.24976/Discov.Med.202537195.58

Celastrol Targets *FANCD2* to Induce Autophagy-Dependent Ferroptosis in Hepatocellular Carcinoma Cells

Jici Yan[1,*], Tian Xu[1]

[1]Department of Interventional Medicine, The People's Hospital of Liaoning Province, 110000 Shenyang, Liaoning, China
*Correspondence: yanjici_yanjc@163.com (Jici Yan)
Published: 20 April 2025

Background: Celastrol has been shown to inhibit hepatocellular carcinoma (HCC) progression, but the underlying mechanism is unknown. Fanconi anemia complementation group D2 (*FANCD2*), a ferroptosis inhibitor, promotes HCC proliferation and invasion. This study aims to investigate whether Celastrol exerts its effects by targeting *FANCD2*.
Methods: Using data from The Cancer Genome Atlas (TCGA), we identified differentially expressed genes in HCC utilizing Gene Expression Profiling Interactive Analysis 2 (GEPIA 2). *FANCD2* and Celastrol were analyzed for molecular docking using Autodock, which was based on geometric matching and energy matching. The correlation between *FANCD2* and survival rate was analyzed using Kaplan-Meier's estimates by log-rank (Mantel-Cox) test. HCC cell lines (SNU-423 and SNU-387) were overexpressed or silenced with *FANCD2* and treated with Celastrol. Autophagy and ferroptosis were evaluated by measuring oxidative stress and related markers, and cell function experiments were performed.
Results: High expression of *FANCD2* was correlated with poor survival in HCC patients. Celastrol targeted *FANCD2*, reducing its level in SNU-423 and SNU-387 cells. *FANCD2* overexpression resulted in increased SNU-423 cell viability, migration, invasion, and tube formation ability, as well as attenuated autophagy and ferroptosis, while *FANCD2* knockdown in SNU-387 cells showed opposite effects. Additionally, *FANCD2* overexpression reversed the ability of Celastrol to induce autophagy and ferroptosis and to inhibit SNU-423 cell survival *in vitro*, while *FANCD2* knockdown enhanced the effects of Celastrol in SNU-387 cells.
Conclusion: Celastrol inhibits malignant behavior in HCC cells by targeting *FANCD2* to induce autophagy-dependent ferroptosis.

Keywords: Celastrol; *FANCD2*; hepatocellular carcinoma; ferroptosis

Introduction

Liver cancer is the second most lethal tumor worldwide, with a 5-year survival rate of 18% [1]. Most primary liver cancers are hepatocellular carcinoma (HCC), which is primarily caused by hepatitis B and C viruses and alcoholism [2]. In recent years, despite significant advances in HCC diagnosis and treatment, including surgical resection, radiation, chemotherapy, and radiofrequency ablation [3], the poor prognosis and high recurrence in HCC patients highlight the need for new, safe, and effective therapies [4].

Ferroptosis, an iron-dependent cell death characterized by lipid peroxidation, is involved in various conditions such as cancer, including HCC [5]. It is defined as an adaptive mechanism that destroys HCC cells [6]. Excessive iron from disrupted redox systems or abnormal iron metabolic processes generates reactive oxygen species (ROS), leading to oxidative stress, lipid peroxidation, and ferroptosis [5,7,8]. Autophagy, a cellular degradation process, results in iron accumulation and ROS production, which further promotes lipid peroxidation to induce ferroptosis [9]. Autophagy-dependent ferroptosis plays a role in HCC treatment [10].

Fanconi anemia complementation group D2 (*FANCD2*), a protein involved in the repair of DNA damage [11], inhibits autophagy-dependent ferroptosis [12,13]. Targeting *FANCD2* to inhibit ferroptosis is considered as a new strategy to reduce the malignancy of glioblastoma cells [14]. Moreover, *FANCD2* is highly expressed in HCC tissues, and the knockdown of *FANCD2* suppresses HCC cell progression by crippling the proliferative and invasive abilities of these cells [15]. Therefore, targeting *FANCD2* may promote autophagy-dependent ferroptosis, thereby limiting HCC progression.

With China attaching great importance to Traditional Chinese Medicine (TCM), the TCM industry has developed rapidly [16]. Celastrol, a pentacyclic triterpene derived from *Tripterygium wilfordii Hook. F.*, is a traditional herbal medicine used to treat autoimmune diseases, cancer, diabetes, and neurodegenerative diseases [17,18]. Celastrol is also an effective drug against HCC, strongly inhibiting proliferation and invasion while inducing HCC cell apopto-

sis [19,20]. A previous study showed that Celastrol inhibits EZrin-mediated HCC migration [21]. Celastrol also mitigates HCC proliferation by indirectly regulating the interaction of the farnesoid X receptor and the retinoid X receptor α *in vivo* and *in vitro* [22]. In the present study, through the bioinformatics tool, Herb, Celastrol was predicted to target *FANCD2*. Because of this, we further speculated that targeting *FANCD2*-induced promotion of autophagy-dependent ferroptosis of HCC cells may serve as the downstream mechanism by which Celastrol contains HCC progression.

In this study, the role of *FANCD2* in modulating autophagy-dependent ferroptosis and malignant behaviors of HCC cells was demonstrated. We also investigated whether and how *FANCD2* expression manipulation affects the tumor-suppressive effect of Celastrol in HCC. Our study aimed to uncover a novel downstream mechanism through which Celastrol suppresses HCC progression.

Materials and Methods

Cell Lines and Drugs

Human HCC cell lines procured from American Type Culture Collection (ATCC, Manassas, VA, USA), including SNU-387 (CRL-2237), SNU-423 (CRL-2238), and human normal hepatocytes (THLE-2; CRL-2706), were grown in Dulbecco's Modified Eagle Medium: F-12 (DMEM/F-12; A4192001, Thermo Fisher Scientific, Waltham, MA, USA) containing 10% fetal bovine serum (FBS; 12103C, Sigma-Aldrich, St Louis, MO, USA) and 1% penicillin-streptomycin (TMS-AB2, Sigma-Aldrich, St. Louis., MO, USA) (temperature, 37 °C; humidity, 5% CO_2). The culture medium was replaced every 2 days. All cells used in this study were mycoplasma negative, and their identity was verified by short tandem repeat (STR) analysis.

Human umbilical vein endothelial cells (HUVECs; PCS-100-01, ATCC, Manassas, VA, USA) were used for the tube formation assay, before which cells were cultured in specific culture medium (CM-0122, Procell Life Science & Technology, Wuhan, China) in 5% CO_2 at 37 °C.

Celastrol in powder form was obtained from Yuanye Bio-Technology (34157-83-0, Shanghai, China) and dissolved in dimethylsulfoxide (DMSO; ST038, Beyotime, Shanghai, China). For Celastrol treatment, SNU-423 and SNU-387 cells were cultured in the presence of different concentrations (1, 2, 4, 8 µmol/L) of Celastrol for 48 h.

Bioinformatics Analyses

In the The Cancer Genome Atlas (TCGA) website, liver hepatocellular carcinoma (LIHC) was searched, followed by selection of RNA-seq data and transcriptome profiling data and addition of cart for downloading mRNA data. Limma was employed to perform gene differential expression analysis in HCC. *FANCD2* expression in HCC and normal specimens, along with the association between *FANCD2* expression and HCC patient survival (log-rank [Mantel-Cox] test), both underwent dissection by Gene Expression Profiling Interactive Analysis 2 (GEPIA 2; http://gepia2.cancer-pku.cn/#survival). Autodock (https://autodock.scripps.edu) was used to predict the three-dimensional structure of the docking of *FANCD2* with Celastrol.

Transfection

The sequences of *FANCD2* used for overexpression are listed in **Supplementary File 1**. The *FANCD2* overexpression plasmid, empty plasmid (negative control, NC), small interfering RNA (siRNA, 5′-AGAAGCTCTTTCAGACCCTG-3′) for *FANCD2*, and siRNA-negative control (siNC, 5′-GTTCCGCGTTACATAACTTA-3′) were prepared by Genepharma (Shanghai, China). SNU-423 and SNU-387 cells underwent transfection of *FANCD2* and NC or si*FANCD2* and siNC, respectively. In brief, 2×10^5 cells/mL cells in a 6-well plate were cultured in 2 mL medium. When the confluence of cells reached 80%, 2 µg of plasmid and 3 µL of Lipofectamine 3000 Transfection Reagent (L3000001, Thermo Fisher Scientific, Waltham, MA, USA) were added to cells at 37 °C for 48 h for transfection. Cells were later collected for analysis or further treated with Celastrol.

Cell Counting Kit-8 (CCK-8) Assay

The viability of the transfected SNU-423 and SNU-387 cells in complete medium for 0, 24, and 48 h was determined using a CCK-8 Kit (C0037, Beyotime, Shanghai, China). In brief, 100 µL of adherent cells (5×10^4 cells/mL) in a 96-well plate were incubated with 10 µL of CCK-8 solution for 1 h at 37 °C. Subsequently, the optical density (OD) at 450 nm was read by a microplate reader (Fluoroskan Ascent, Thermo Fisher Scientific, Waltham, MA, USA).

Cell Apoptosis Assay

Apoptosis of SNU-423 and SNU-387 cells after transfection and/or Celastrol treatment was measured using an Annexin V-FITC Apoptosis Detection Kit (C1062, Beyotime, Shanghai, China). After digesting with trypsin and washing with phosphate-buffered saline (PBS; C0221A, Beyotime, Shanghai, China), 5×10^4 cells were stained with 195 µL of Annexin V-FITC binding buffer together with 5 µL of Annexin V-FITC and 10 µL of propidium iodide (PI) in darkness for 15 min. Apoptosis was evaluated using a flow cytometer (BD FACSCalibur, Becton-Dickinson, Franklin, NJ, USA), and data were analyzed using FlowJo software (VX10, Tree Star, Ashland, OR, USA).

ROS Production Assessment

A 2′,7′-Dichlorodihydrofluorescein diacetate (DCFDA)-Cellular ROS Assay Kit (ab113851, Ab-

cam, Cambridge, MA, USA) was used to measure ROS production in SNU-423 and SNU-387 cells. After transfection and/or Celastrol treatment, SNU-423 or SNU-387 cells in a 96-well plate (2.5×10^4 cells/well) were cultured to be adherent to the plates, after which 100 µL of diluted DCFDA solution was added to each well for 45 min. Cells were rinsed with buffer and observed with a fluorescent microscope (BX63, Olympus, Tokyo, Japan) at ×200 magnification.

Malondialdehyde (MDA), Superoxide Dismutase (SOD), Glutathione (GSH), and Iron Level Determination

SNU-423 and SNU-387 cells that underwent transfection and/or Celastrol treatment were subjected to colorimetric assays, in which MDA, SOD, GSH, and iron ion levels were determined in 96-well plates with an MDA/SOD Assay Kit (ab118970/ab65354, Abcam, Cambridge, MA, USA) or a GSH/Iron Assay Kit (E2015/E1042, Applygen Technologies, Beijing, China).

For the MDA assay, cells (2.5×10^6) were lysed with MDA lysis buffer and reacted with 600 µL of TBA reagent (95 °C, 60 min). Cells were then cooled to room temperature, followed by detection at 532 nm using a microplate reader (iMark, Beyotime, Shanghai, China).

For the SOD assay, cells (2.5×10^6) were lysed with lysis buffer (P0013J, Beyotime, Shanghai, China), which were then combined with water-soluble tetrazolium salt (WST) working solution (200 µL/well) and enzyme working solution (20 µL/well). After mixing, cells were incubated (20 min, 37 °C), followed by detection at 450 nm using a microplate reader (iMark, Beyotime, Shanghai, China).

For the GSH assay, 10 µL homogenate or standards, 10 µL protein removal reagent S solution and with 150 µL total glutathione detection working solution sequentially added to each well of a 96-well plate (room temperature, 2 min), and then with 50 µL of nicotinamide adenine dinucleotide phosphate (NADPH) working solution (20 min, 25 °C). Subsequently, the wells were detected at 412 nm using a microplate reader (iMark, Beyotime, Shanghai, China).

For the iron assay, 100 µL of cell lysate was reacted with 100 µL of reaction mix (60 °C, 1 h) and then with 30 µL of iron ion detector (60 min), followed by detection at 550 nm using a microplate reader (iMark, Beyotime, Shanghai, China).

Tube Formation Assay

Each well of the µ-Slide (81506, IBIDI, Martinsried, Germany) was coated with 10 µL of Matrigel (356231, BD Biosciences, Franklin Lakes, NJ, USA), bubbles were removed by low-speed aseptic centrifugation, and plates were incubated at 37 °C for 30–60 min. HUVECs were digested with 0.25% trypsin and resuspended in culture supernatants of SNU-423 and SNU-387 cells, which were previously subjected to transfection and/or Celastrol treatment. HUVECs were then seeded onto a layer of SNU-423 cells that underwent transfection and Celastrol treatment. The conditioned medium was collected. Next, HUVECs were seeded onto Matrigel (3×10^4 cells/well). After culture in the conditioned medium for 4 h, the medium from the upper chamber was removed and 50 µL of calcein diluted in serum-free medium (6.25 µg/mL, HY-D0040, MedChemExpress, Shanghai, China) was added, followed by incubation at room temperature for 30 min in darkness. The capillary-like structures were captured by a fluorescence microscope (Nikon E800 Fluorescence Microscope, Nikon, El Segundo, CA, USA) at 200× magnification. The length, covering area, and branch points of the capillary-like tubes were measured and counted.

Cell Scratch Assay

After transfection and/or Celastrol treatment, SNU-423 and SNU-387 cells were processed for the cell scratch assay to assess their migratory ability. Cells in a 6-well plate (2×10^4 cells/well) were cultured to 95% confluence. A vertical scratch was created with a sterile pipette tip, and cell debris was removed by rinsing with PBS. At 0 and 24 h of incubation with Celastrol, cell images in the scratch area were obtained with an optical microscope (Axiolab 5, Zeiss, Oberkochen, Germany) at 100× magnification. Each experiment was performed in triplicate.

Transwell Assay

After transfection and/or Celastrol treatment, SNU-423 and SNU-387 cells were digested and washed with 0.25% trypsin (C0201) and PBS (C0221A; twice) obtained from Beyotime (Shanghai, China), respectively. Cells (3×10^5 cells/mL) were suspended in serum-free medium (A4192001, Thermo Fisher Scientific, Waltham, MA, USA). Next, 100 µL of the cell suspension was added to the upper Matrigel-coated chamber, and 500 µL of complete medium was added to the lower chamber. Cells remaining in the upper chamber were removed by cotton swabs, and invaded cells were fixed (4% paraformaldehyde, 8.18715, Sigma-Aldrich, St Louis, MO, USA), stained (0.1% crystal violet, R40052, Thermo Fisher Scientific, Waltham, MA, USA), and counted under a microscope (Axiolab 5, Zeiss, Oberkochen, Germany) at 100× magnification.

Quantitative Reverse Transcription-Polymerase Chain Reaction (qRT-PCR)

The total RNA extracted from HCC/adjacent tissue specimens or cells harvested after transfection and/or Celastrol treatment was processed for qRT-PCR. HCC tissue specimens and cells were digested with 1 mL of TRIzol reagent (15596026, Thermo Fisher Scientific, Waltham, MA, USA). The isolated RNA was diluted with 200 µL of trichloromethane (T117625, Aladdin, Shanghai, China)

Table 1. Primer sequences for qRT-PCR.

Primer name	Primer sequence (5′-3′)
FANCD2-F	AAAACGGGAGAGAGTCAGAATCA
FANCD2-R	ACGCTCACAAGACAAAAGGCA
Bcl-2-F	GTGGAGGAGCTCTTCAGGGA
Bcl-2-R	AGGCACCCAGGGTGATGCAA
Bax-F	GGCCCACCAGCTCTGAGCAGA
Bax-R	GCCACGTGGGCGTCCCAAAGT
GAPDH-F	GGAGCGAGATCCCTCCAAAAT
GAPDH-R	GGCTGTTGTCATACTTCTCATGG

FANCD2, Fanconi anemia complementation group D2; *Bcl-2*, B-cell lymphoma-2; *Bax*, Bcl-2-associated X protein; *GAPDH*, glyceraldehyde-3-phosphate dehydrogenase; F, Forward; R, Reverse; qRT-PCR, Quantitative Reverse Transcription-Polymerase Chain Reaction.

and incubated for 5 min. The reaction mixture was centrifuged (12,000 rpm, 20 min, 4 °C), and RNA was precipitated with 1 mL of isopropyl alcohol (9500-1, Thermo Fisher Scientific, Waltham, MA, USA). RNA was dissolved in DEPC-treated water (750024, Thermo Fisher Scientific, Waltham, MA, USA) and reverse-transcribed using a PrimeScript RT reagent Kit (RR037A, Takara, Tokyo, Japan). In brief, 5×PrimeScript Buffer, PrimeScript RT Enzyme Mix I, RT Primer Mix, and RNase Free dH_2O were combined with RNA to synthesize cDNA. Subsequently, PCR amplification was performed by a TB Green Premix Ex Taq™ II (RR820A, Takara, Tokyo, Japan): TB Green Premix Ex Taq II, ROX Reference Dye II, appropriate primer, cDNA, DEPC-treated water, and primer sequences (Table 1) were mixed uniformly, the mixture was added into Applied Biosystems 7500 Fast Dx Real-Time PCR Instrument (Thermo Fisher Scientific, Waltham, MA, USA). Amplification was performed at 95 °C (30 s), followed by 40 cycles at 95 °C (5 s) and 60 °C (30 s). Gene quantification was performed using the $2^{-\Delta\Delta Ct}$ method [23].

Western Blot Assay

Protein expression in HCC/adjacent tissue specimens and cells after transfection and/or Celastrol treatment was quantitated by western blot. Following protein extraction (lysis buffer) and concentration determination (BCA assay kit, P0012, Beyotime, Shanghai, China), 20 µL of proteins were loaded on 10% SDS polyacrylamide gel (P0012AC, Beyotime, Shanghai, China), electrophoresed, and transferred to polyvinylidene fluoride (PVDF) membranes (FFP26, Beyotime, Shanghai, China). Membranes were immersed into 5% non-fat milk (1 h, 37 °C) for blocking, incubated with primary antibodies (overnight, 4 °C), washed with TBST (91414, Sigma-Aldrich, St. Louis., MO, USA), and incubated with secondary antibodies (room temperature, 2 h). The antibodies (Abcam, Cambridge, MA, USA) were as follows: FANCD2 (ab108928, 1:1000, 155 kDa), Beclin (ab207612, 1:2000, 52 kDa), light chain 3 (LC3)BII/LC3BI (ab192890, 1:2000, 14/16 kDa), B-cell lymphoma-2 (Bcl-2, ab59348, 1:1000, 26 kDa), Bcl-2-associated X protein (Bax, ab32503, 1:2000, 21 kDa), Cleaved Caspase-3 (ab2302, 1:1000, 17 kDa), glyceraldehyde-3-phosphate dehydrogenase (GAPDH, ab8245, 1:20,000, 36 kDa), and goat anti-rabbit/mouse IgG H&L (HRP) (ab205718/ab205719, 1:2000/1:5000). Immunoreactivity was detected with an enhanced chemiluminescence (ECL) kit (P0018, Beyotime, Shanghai, China) and a chemiluminescence imaging system (ChemiDoc XRS+, Bio-Rad, Hercules, CA, USA). Band densities were analyzed by software (Image J 1.5i, National Institutes of Health, Bethesda, MD, USA). All protein expression levels were normalized against GAPDH.

Statistical Analysis

Mean ± SD was used to depict all values. One-way analysis of variance (ANOVA) test was performed to compare means between multiple groups. All analyses were performed by GraphPad Prism (version 8, GraphPad Software, San Diego, CA, USA). p value < 0.05 indicated a statistically significant difference.

Results

FANCD2 was Highly Expressed in HCC

Using limma based on the mRNA data downloaded from TCGA, we performed gene differential expression analysis. The results were visualized through a volcano plot (Fig. 1A) and a heat map (Fig. 1B), which displayed that the HCC specimens harbored upregulated and downregulated mRNAs. Compared to the normal tissues, *FANCD2* expression was among the upregulated mRNAs in the HCC specimens (Fig. 1C, $p < 0.05$).

FANCD2 was Downregulated by Celastrol in HCC Cells where Highly Expressed FANCD2 was Detected and Associated With Poor Survival of HCC Patients

Molecular docking analysis using Autodock illustrated that *FANCD2* can dock with Celastrol (Fig. 2A). To investigate the effect of Celastrol on the expression of *FANCD2* in HCC, qRT-PCR was performed using Celastrol (1, 2, 4, and 8 µM)-treated SNU-423 and SNU-387 cells. SNU-423 and SNU-387 cells that were treated with Celastrol (2, 4, and 8 µM) exhibited reduced *FANCD2* expression ($p < 0.05$, Fig. 2B,C). Next, HCC patients were dichotomized into two groups, namely patients with low *FANCD2* expression and patients with high *FANCD2* expression, according to the cut-off value, the median of *FANCD2* expression. Kaplan-Meier's estimates showed that high *FANCD2* expression was associated with shorter survival time of HCC patients, compared to low *FANCD2* expression ($p = 0.0051$, Fig. 2D).

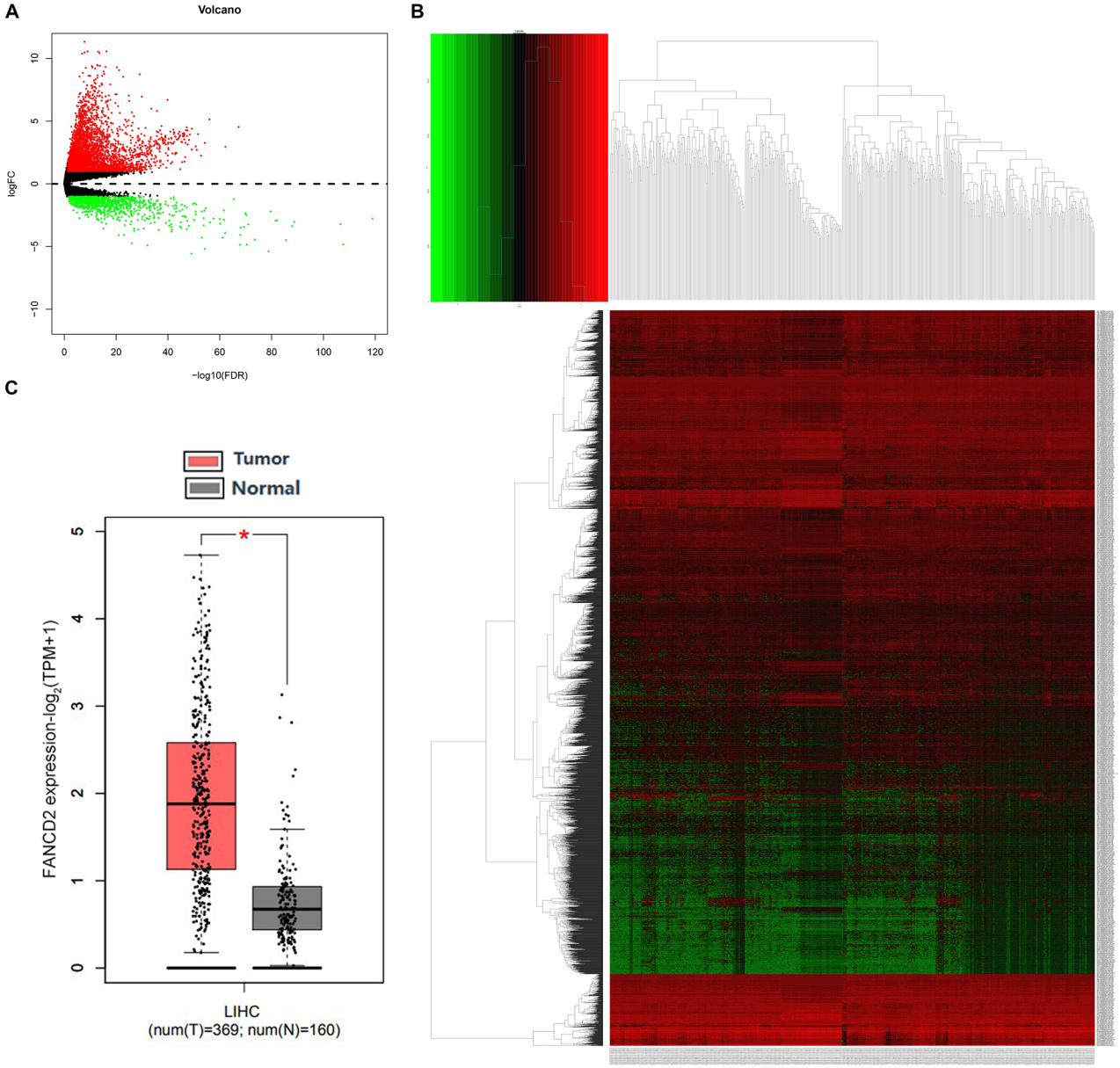

Fig. 1. *FANCD2* was highly expressed in HCC. (A,B) Based on data from TCGA, limma was used to analyze differentially expressed mRNAs in HCC, and these mRNAs were visualized in a volcano plot (A) and a heat map (B), red: upregulation; green: downregulation. (C) Prediction on *FANCD2* expression in HCC (T, red) and normal samples (N, gray) (Gene Expression Profiling Interactive Analysis 2 (GEPIA 2), http://gepia2.cancer-pku.cn/#survival). *$p < 0.001$, vs. normal samples. HCC, hepatocellular carcinoma; TCGA, The Cancer Genome Atlas; GEPIA 2, Gene Expression Profiling Interactive Analysis 2.

FANCD2 Expression was Altered in HCC Cells

In line with qRT-PCR results, *FANCD2* expression was higher in SNU-387 and SNU-423 cells than in THLE-2 cells ($p < 0.001$, Fig. 2E). SNU-423 cells were transfected with *FANCD2* overexpression plasmids, and SNU-387 cells were transfected with si*FANCD2*. FANCD2 protein and mRNA expression levels were increased in SNU-423 cells after *FANCD2* overexpression plasmid transfection ($p < 0.001$, Fig. 3A–C), while transfection with si*FANCD2* led to decreased FANCD2 protein and mRNA expression levels in SNU-387 cells ($p < 0.001$, Fig. 3D–F).

FANCD2 Positively Modulated HCC Cell Viability and Negatively Impacted HCC Cell Apoptosis Induced by Celastrol

Cell viability was measured with the CCK-8 assay. At 48 h after transfection, the OD value was higher in SNU-423 cells overexpressing *FANCD2* compared to NC-transfected SNU-423 cells ($p < 0.01$, Fig. 4A), but was lower in SNU-387 cells transfected with si*FANCD2* compared to siNC-transfected SNU-387 cells ($p < 0.01$, Fig. 4B). Flow cytometry analysis revealed that treatment with Celastrol (4 μM, used in the following experiments,

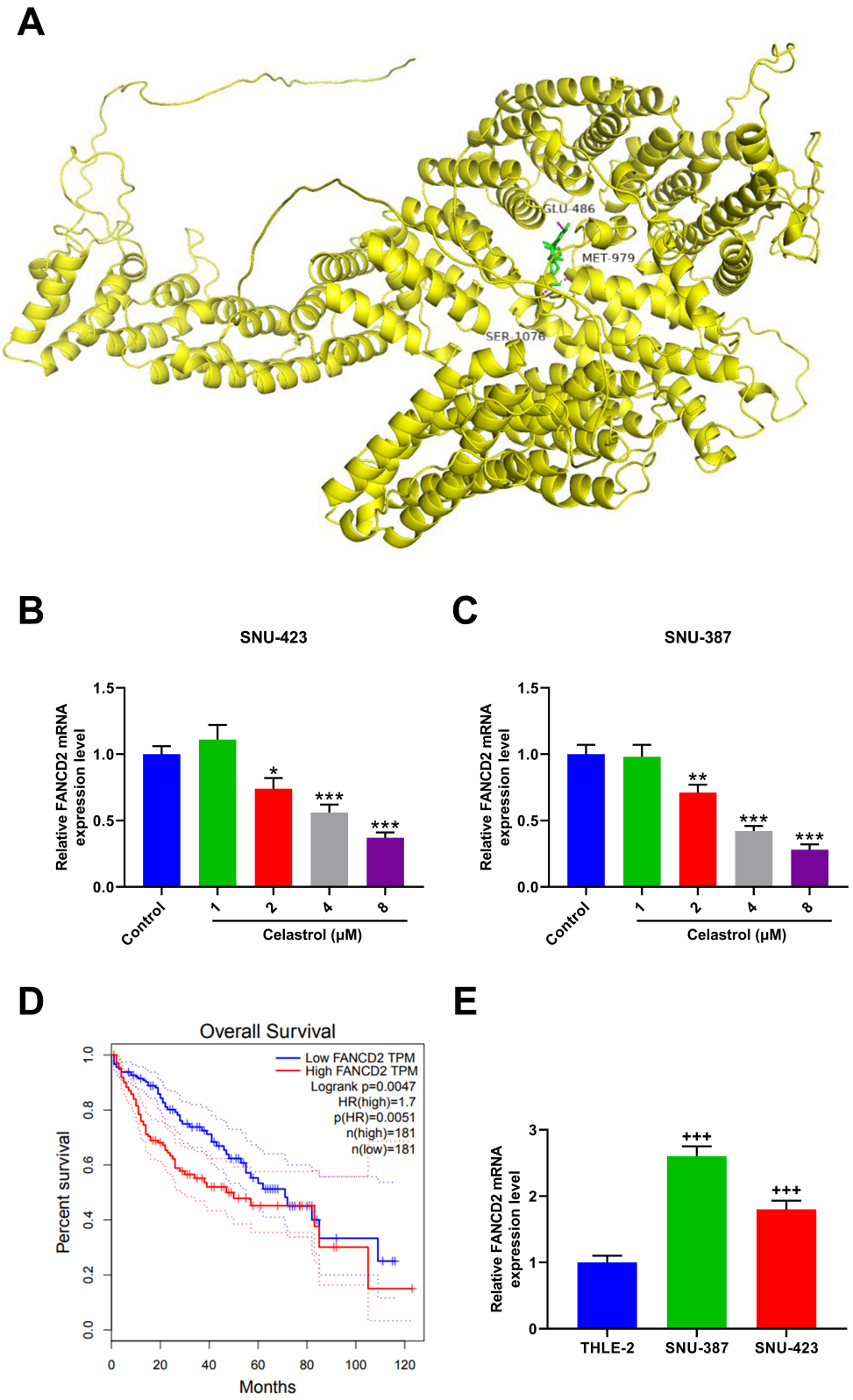

Fig. 2. *FANCD2* was downregulated by Celastrol in HCC cells where highly expressed *FANCD2* was detected and associated with poor survival of HCC patients. (A) Autodock (https://autodock.scripps.edu) was used to predict the three-dimensional structure of the docking of *FANCD2* genes treated with Celastrol. (B,C) *FANCD2* expression in SNU-423 and SNU-387 cells after Celastrol (1, 2, 4, 8 μM) treatment (qRT-PCR). (D) Analysis of the association between *FANCD2* and HCC patient survival (GEPIA 2, http://gepia2.cancer-pku.cn/#survival). (E) *FANCD2* expression in THLE-2, SNU-387, and SNU-423 cells (qRT-PCR, *GAPDH* as the internal reference). $^{*}p < 0.05$, $^{**}p < 0.001$, $^{***}p < 0.001$, vs. Control; $^{+++}p < 0.001$, vs. THLE-2. n = 3.

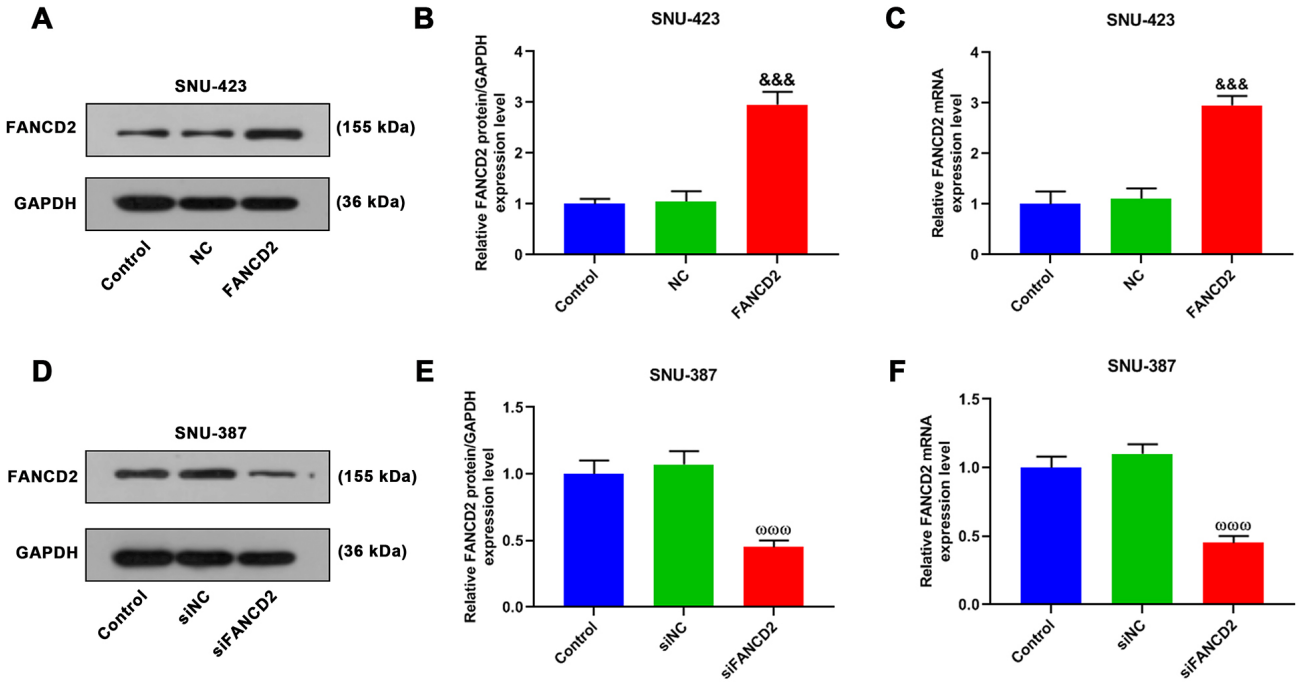

Fig. 3. FANCD2 expression was altered in HCC cells. (A–F) FANCD2 expression in SNU-423 cells transfected with NC or *FANCD2* plasmids and in SNU-387 cells transfected with siNC or si*FANCD2* (western blot (A,B,D,E) and qRT-PCR (C,F), GAPDH as the internal reference). $^{\&\&\&}p < 0.001$, vs. NC; $^{\omega\omega\omega}p < 0.001$, vs. siNC. n = 3. NC, negative control; siNC, small interfering RNA for NC.

as it is closest to the half maximal inhibitory concentration of Celastrol for HCC cells) caused SNU-423 cell apoptosis promotion and SNU-387 cell apoptosis promotion ($p < 0.001$, Fig. 4C–E), which were attenuated by *FANCD2* overexpression ($p < 0.001$, Fig. 4C,E) and potentiated by *FANCD2* knockdown ($p < 0.001$, Fig. 4D,E). *FANCD2* knockdown, compared to siNC transfection, facilitated SNU-387 cell apoptosis ($p < 0.001$, Fig. 4D,E).

Celastrol Downregulated FANCD2 to Promote ROS Production in HCC Cells

In both SNU-423 and SNU-387 cells, ROS levels increased after Celastrol treatment, and *FANCD2* overexpression weakened the effect of Celastrol on ROS production in SNU-423 cells, whereas *FANCD2* knockdown potentiated the effect in SNU-387 cells ($p < 0.001$, Fig. 5A–C).

Celastrol Downregulated FANCD2 to Facilitate Ferroptosis and Autophagy in HCC Cells

The levels of proteins related to ferroptosis were assessed in HCC cells after transfection and/or Celastrol treatment. *FANCD2* overexpression had no effect on the level of MDA but increased SOD and GSH levels in SNU-423 cells ($p < 0.05$, Fig. 6A–C). In contrast, MDA levels increased but SOD and GSH levels decreased in SNU-387 cells after *FANCD2* knockdown ($p < 0.05$, Fig. 6E–G). However, both *FANCD2* overexpression and *FANCD2* knockdown did not affect the levels of iron in SNU-423 and SNU-387 cells (Fig. 6D,H). Celastrol treatment increased MDA and iron levels, while decreasing SOD and GSH levels in both SNU-423 and SNU-387 cells ($p < 0.001$, Fig. 6A–H). The effect of Celastrol on the levels of the ferroptosis-related molecules mentioned above was neutralized by *FANCD2* overexpression ($p < 0.05$, Fig. 6A–D) but was potentiated by *FANCD2* knockdown ($p < 0.05$, Fig. 6E–H).

In HCC cells, after transfection and/or Celastrol treatment, the expression levels of autophagy-related molecules were examined. The expression of Beclin, LC3BII, and LC3BII/LC3BI decreased, while the expression of LC3BI increased after *FANCD2* overexpression in SNU-423 cells ($p < 0.05$, Fig. 6I–K). *FANCD2* knockdown in SNU-387 cells increased the expressions of Beclin, LC3BII, and LC3BII/LC3BI, while diminishing the expression of LC3BI ($p < 0.05$, Fig. 6L–N). Both SNU-423 and SNU-387 cells treated with Celastrol exhibited increased expressions of Beclin, LC3BII, and LC3BII/LC3BI, and decreased LC3BI expression ($p < 0.01$, Fig. 6I–N). *FANCD2* overexpression offset the effect of Celastrol on the expressions of these autophagy-related molecules in SNU-423 cells ($p < 0.01$, Fig. 6I–K), but *FANCD2* knockdown strengthened the effect in SNU-387 cells ($p < 0.01$, Fig. 6L–N).

Celastrol Downregulated FANCD2 to Inhibit Tube Formation Induced by HCC Cells

The results of the tube formation assay are shown in Fig. 7A–C. *FANCD2* overexpression promoted the ability of SNU-423 cells to form HUVEC tubes ($p < 0.05$, Fig. 7A,B). On the contrary, *FANCD2* knockdown

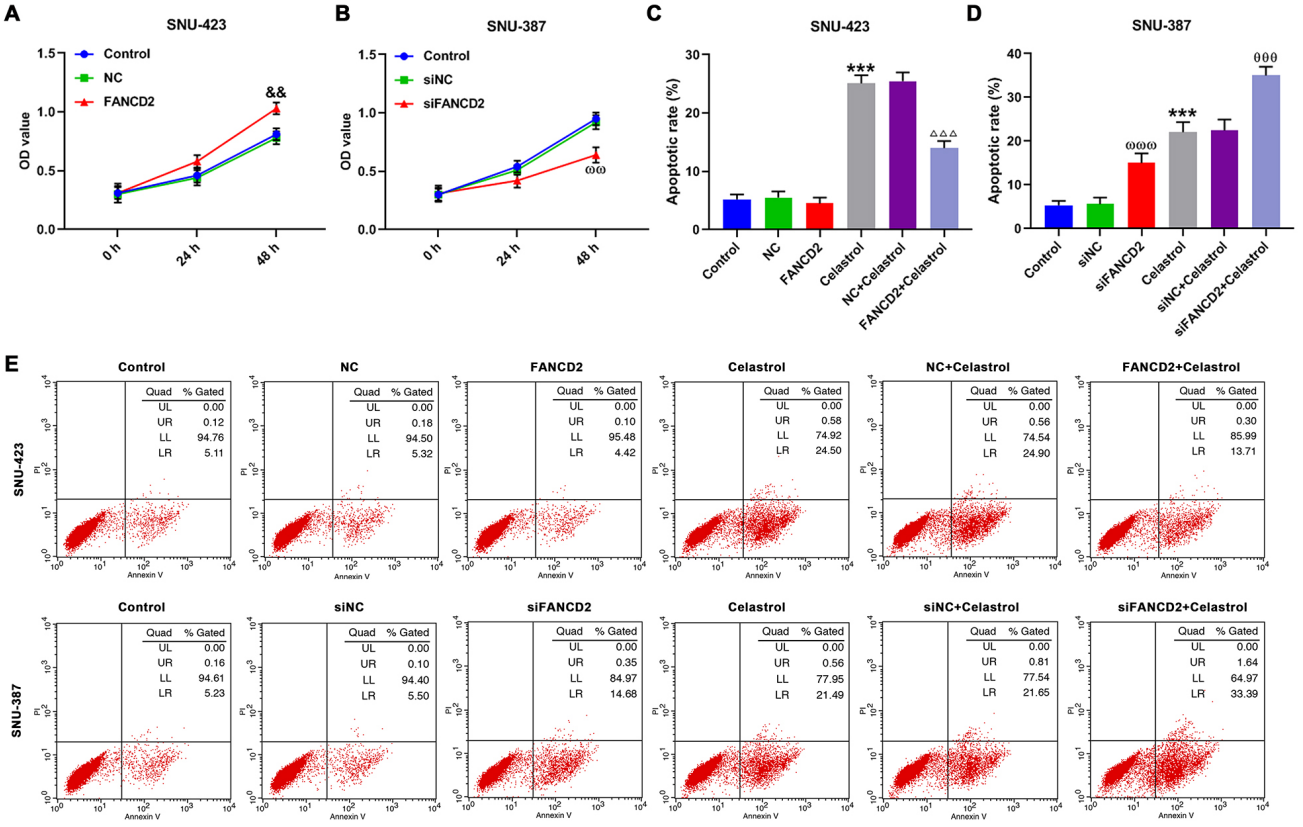

Fig. 4. *FANCD2* positively modulated HCC cell viability and negatively impacted HCC cell apoptosis induced by Celastrol. (A,B) Viability of SNU-423 cells transfected with NC or *FANCD2* plasmids and that of SNU-387 cells transfected with siNC or si*FANCD2* (Cell Counting-Kit-8 assay). (C–E) Apoptosis of SNU-423 cells transfected with NC/*FANCD2* plasmids and treated with Celastrol (4 μM) and that of SNU-387 cells transfected with siNC/ si*FANCD2* and treated with Celastrol (4 μM) (flow cytometry). $^{\&\&}p < 0.001$, vs. NC; $^{\omega\omega}p < 0.01$, $^{\omega\omega\omega}p < 0.001$, vs. siNC; ***$p < 0.001$, vs. Control; $^{\triangle\triangle\triangle}p < 0.001$, vs. NC+Celastrol; $^{\theta\theta\theta}p < 0.001$, vs. siNC+Celastrol. n = 3. si*FANCD2*, small interfering RNA for *FANCD2*.

weakened the ability of SNU-387 cells to form HUVEC tubes ($p < 0.05$, Fig. 7A,C). In addition, it was observed that Celastrol treatment weakened the ability of SNU-423 and SNU-387 cells to form HUVEC tubes ($p < 0.001$, Fig. 7A–C). *FANCD2* overexpression abolished the Celastrol-induced destruction of HUVEC tubes treated with SNU-423 cell-conditioned medium ($p < 0.001$, Fig. 7A,B), while *FANCD2* knockdown potentiated the Celastrol-induced destruction of HUVEC tubes treated with SNU-387 cell-conditioned medium ($p < 0.05$, Fig. 7A,C).

Celastrol Downregulated FANCD2 to Inhibit HCC Cell Migration and Invasion

In the cell scratch assay, *FANCD2* overexpression increased the rate of gap closure in SNU-423 cells ($p < 0.01$, Fig. 8A,B), while *FANCD2* knockdown decreased the rate of the gap closure in SNU-387 cells ($p < 0.001$, Fig. 8A,C). Celastrol treatment inhibited SNU-423 and SNU-387 cell migration ($p < 0.001$, Fig. 8A–C). Moreover, *FANCD2* overexpression counteracted the Celastrol-induced inhibition on SNU-423 cell migration ($p < 0.01$, Fig. 8A,B), while *FANCD2* knockdown intensified the Celastrol-induced inhibition on SNU-387 cell migration ($p < 0.001$, Fig. 8A,C). Transwell invasion assay showed similar results. The invasion rate of *FANCD2*-overexpressed SNU-423 cells was higher than that of NC-transfected cells ($p < 0.01$, Fig. 8D,F), while *FANCD2* knockdown compared to siNC transfection, decreased the invasion rate of SNU-387 cells ($p < 0.001$, Fig. 8E,F). Celastrol treatment inhibited the invasive ability of SNU-423 and SNU-387 cells ($p < 0.001$, Fig. 8D–F). In addition, *FANCD2* overexpression attenuated the effect of Celastrol on SNU-423 cell invasion ($p < 0.001$, Fig. 8D,F), while *FANCD2* knockdown potentiated the effect of Celastrol in inhibiting SNU-387 cell invasion ($p < 0.001$, Fig. 8E,F).

Celastrol Modulated the Expressions of Apoptosis-Related Factors in HCC Cells by Negatively Regulating FANCD2 Expression

In both SNU-423 and SNU-387 cells, Celastrol treatment downregulated FANCD2 and Bcl-2 protein and mRNA expression levels ($p < 0.05$, Fig. 9A–F) and upregulated Bax and cleaved caspase-3 protein and mRNA expression levels ($p < 0.001$, Fig. 9A–F). *FANCD2* over-

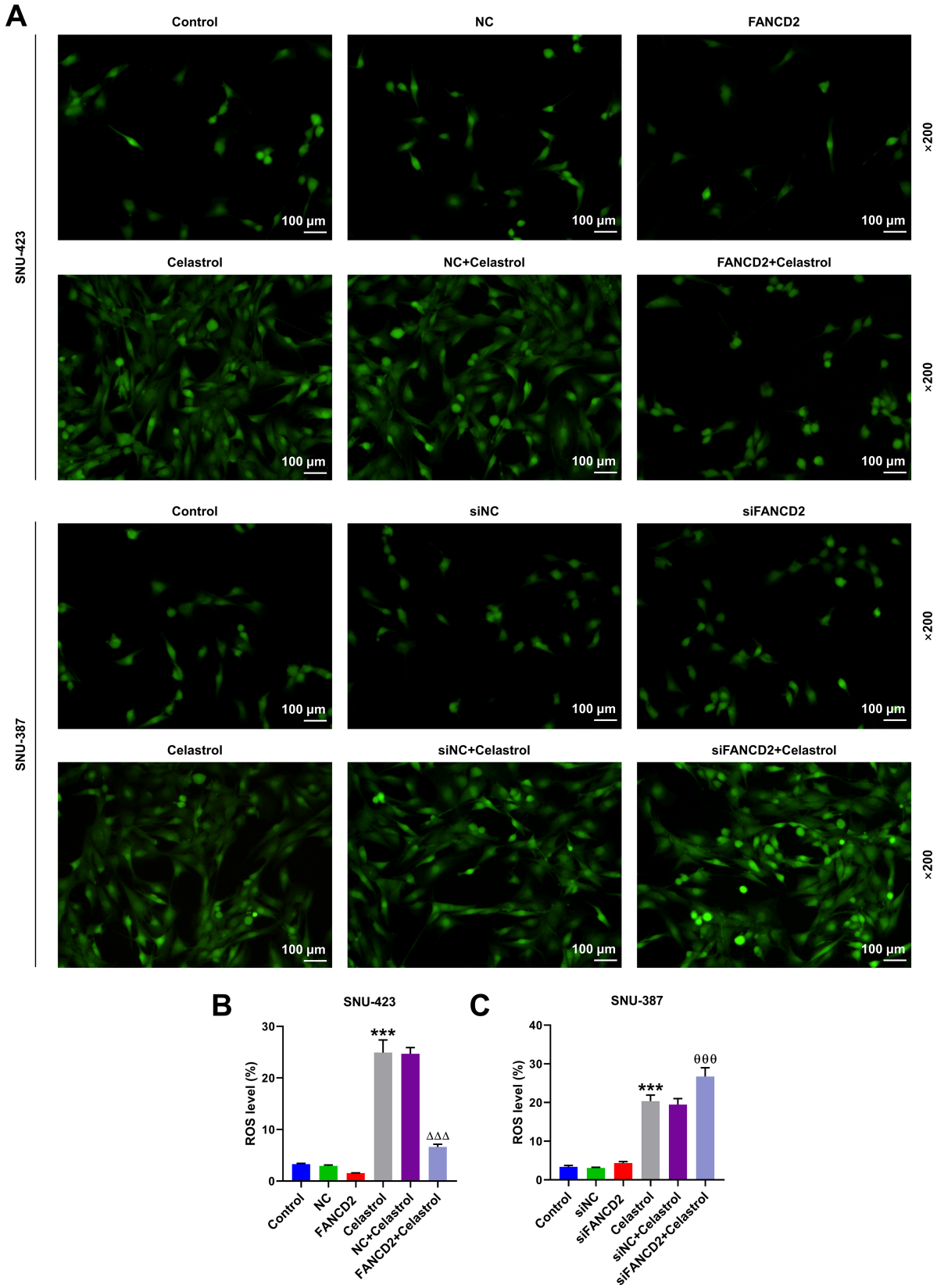

Fig. 5. Celastrol downregulated *FANCD2* to promote ROS production in HCC cells. (A–C) ROS production of SNU-423 cells that were transfected with NC/*FANCD2* plasmids and treated with Celastrol (4 μM) and that of SNU-387 cells that were transfected with siNC/si*FANCD2* and treated with Celastrol (4 μM) were analyzed by the DCFDA method (magnification: ×200; scale bar: 100 μm). ***$p < 0.001$, vs. Control; $^{\triangle\triangle\triangle}p < 0.001$, vs. NC+Celastrol; $^{\theta\theta\theta}p < 0.001$, vs. siNC+Celastrol. n = 3. ROS, reactive oxygen species; DCFDA, 2′,7′-Dichlorodihydrofluorescein diacetate.

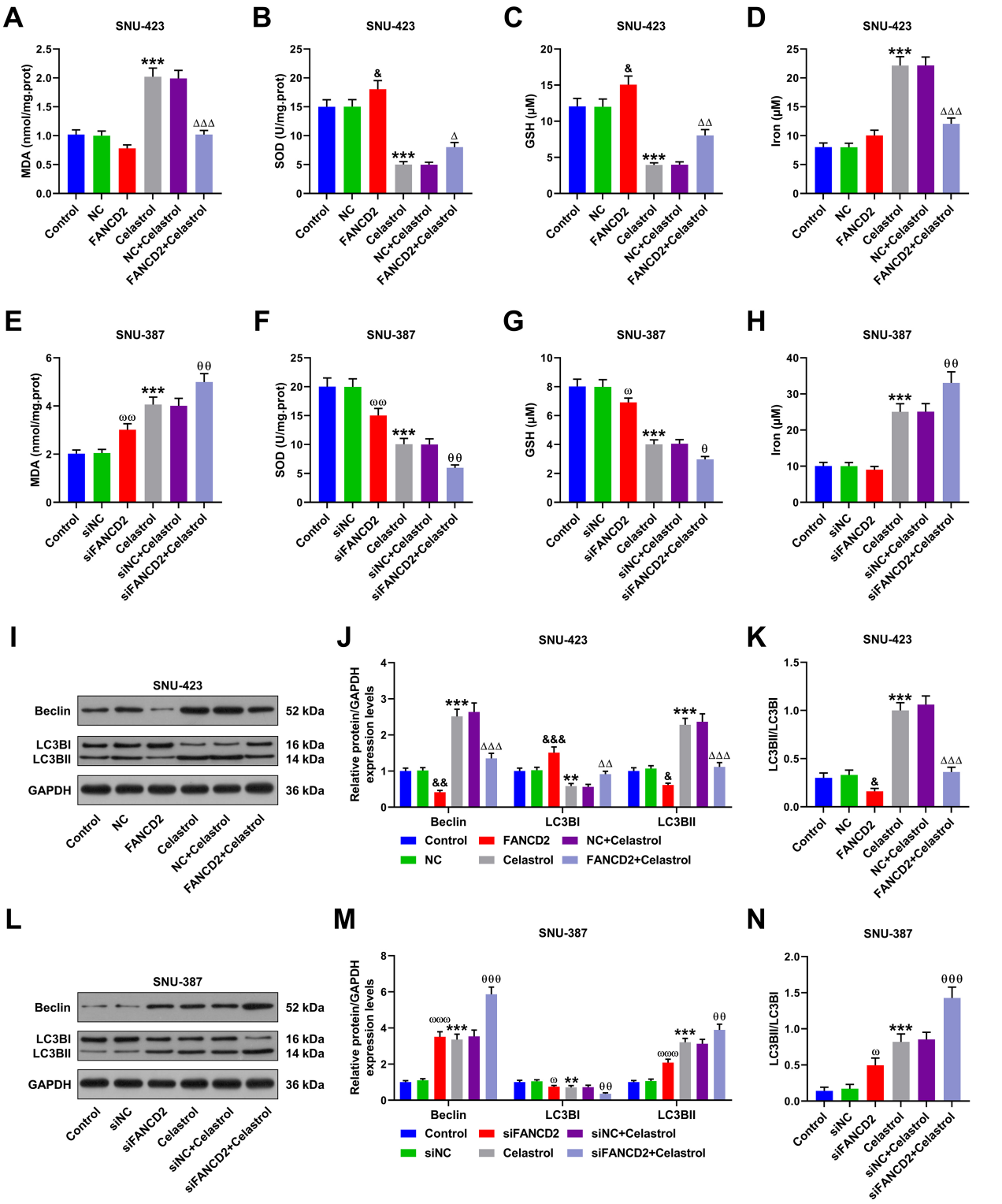

Fig. 6. Celastrol downregulated *FANCD2* to facilitate ferroptosis and autophagy in HCC cells. (A–H) MDA, SOD, GSH, and iron levels in SNU-423 cells transfected with NC/*FANCD2* plasmids and treated with Celastrol (4 μM) and those of SNU-387 cells transfected with siNC/si*FANCD2* and treated with Celastrol (4 μM) (colorimetric assay). (I–N) Beclin, LC3BI, LC3BII, and LC3BII/LC3BI expression levels in SNU-423 cells transfected with NC/*FANCD2* plasmids and treated with Celastrol (4 μM) and those in SNU-387 cells transfected with siNC/si*FANCD2* and treated with Celastrol (4 μM) (western blot, GAPDH as an internal reference). $^{\&}p < 0.05$, $^{\&\&}p < 0.01$, $^{\&\&\&}p < 0.001$, vs. NC; $^{\omega}p < 0.05$, $^{\omega\omega}p < 0.01$, $^{\omega\omega\omega}p < 0.001$, vs. siNC; $^{**}p < 0.01$, $^{***}p < 0.001$, vs. Control; $^{\triangle}p < 0.05$, $^{\triangle\triangle}p < 0.01$, $^{\triangle\triangle\triangle}p < 0.001$, vs. NC+Celastrol; $^{\theta}p < 0.05$, $^{\theta\theta}p < 0.01$, $^{\theta\theta\theta}p < 0.001$, vs. siNC+Celastrol. n = 3. MDA, malondialdehyde; SOD, superoxide dismutase; GSH, glutathione; LC3, light chain 3.

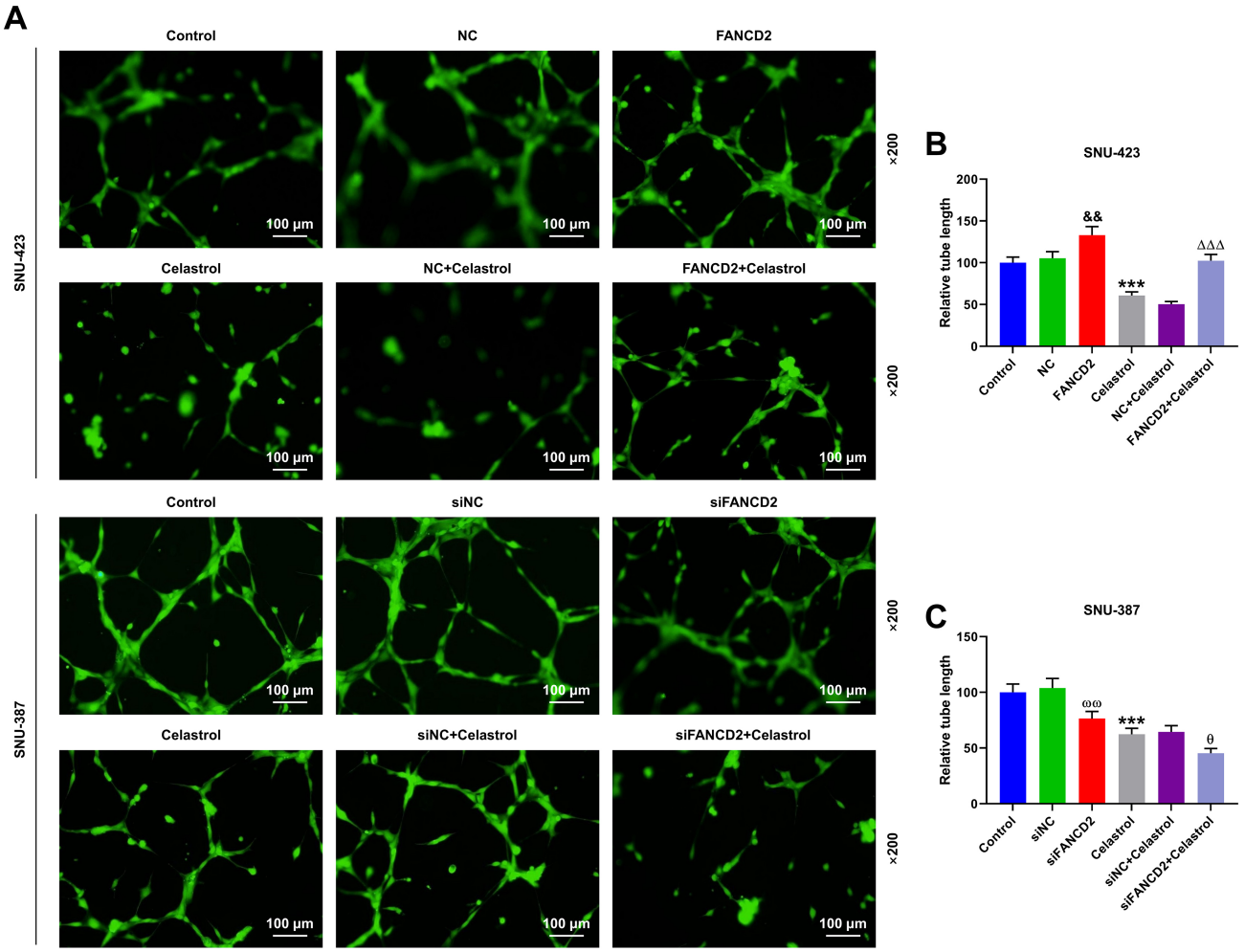

Fig. 7. Celastrol downregulated *FANCD2* to inhibit tube formation induced by HCC cells. (A–C) Tube formation ability of SNU-423 cells after *FANCD2* plasmid/NC transfection and/or Celastrol (4 μM) treatment and that of SNU-387 cells after si*FANCD2*/siNC transfection and/or Celastrol (4 μM) treatment to form capillary-like tubes (tube formation assay) (magnification: ×200; scale bar: 100 μm). $^{\&\&}p < 0.01$, vs. NC; $^{\omega\omega}p < 0.01$, vs. siNC; $^{***}p < 0.001$, vs. Control; $^{\triangle\triangle\triangle}p < 0.001$, vs. NC+Celastrol; $^{\theta}p < 0.05$, vs. siNC+Celastrol. n = 3.

expression had effects opposite to the role of Celastrol on FANCD2 and cleaved caspase-3 expression in SNU-423 cells ($p < 0.05$, Fig. 9A–C), and no effects on Bax and Bcl-2 expression (Fig. 9A–C). The effect of Celastrol on FANCD2, Bax, Bcl-2, and cleaved caspase-3 expression in SNU-387 cells ($p < 0.05$, Fig. 9D–F) was similar to that of *FANCD2* knockdown. Moreover, the effects of Celastrol on FANCD2, Bax, Bcl-2 and cleaved caspase-3 expressions were offset by *FANCD2* overexpression in SNU-423 cells ($p < 0.05$, Fig. 9A–C), but were strengthened by *FANCD2* knockdown in SNU-387 cells ($p < 0.05$, Fig. 9D–F).

Discussion

HCC, which accounts for the majority of liver cancers, is the fourth leading cause of cancer-related mortality [24]. Unlike traditional methods, such as surgical resection and conventional chemotherapy, which often cause significant pain and have high recurrence rates and low surgical survival rates [25], Celastrol, a naturally occurring pentacyclic chemical compound, exerts an anti-HCC effect with minimal adverse effects and high efficacy [19]. However, the mechanism by which Celastrol achieves this effect is not fully understood.

Ferroptosis, an iron-dependent form of regulated cell death, primarily affects the cells deficient in critical nutrients or susceptible to infection or ambient stress [26]. Cancer cells exist in a state of constant oxidative stress; however, the delicate balance between thiols and catalytic iron they harbor deters the occurrence of ferroptosis during cancer development [27]. Therefore, ferroptosis is exogenously triggered for therapeutic benefits in cancer [28]. Celastrol can induce ferroptosis in non-small-cell lung cancer (NSCLC) cells, demonstrating its potential anticancer activity [29]. In our study, bioinformatics predictions based on Autodock illustrated that Celastrol can dock

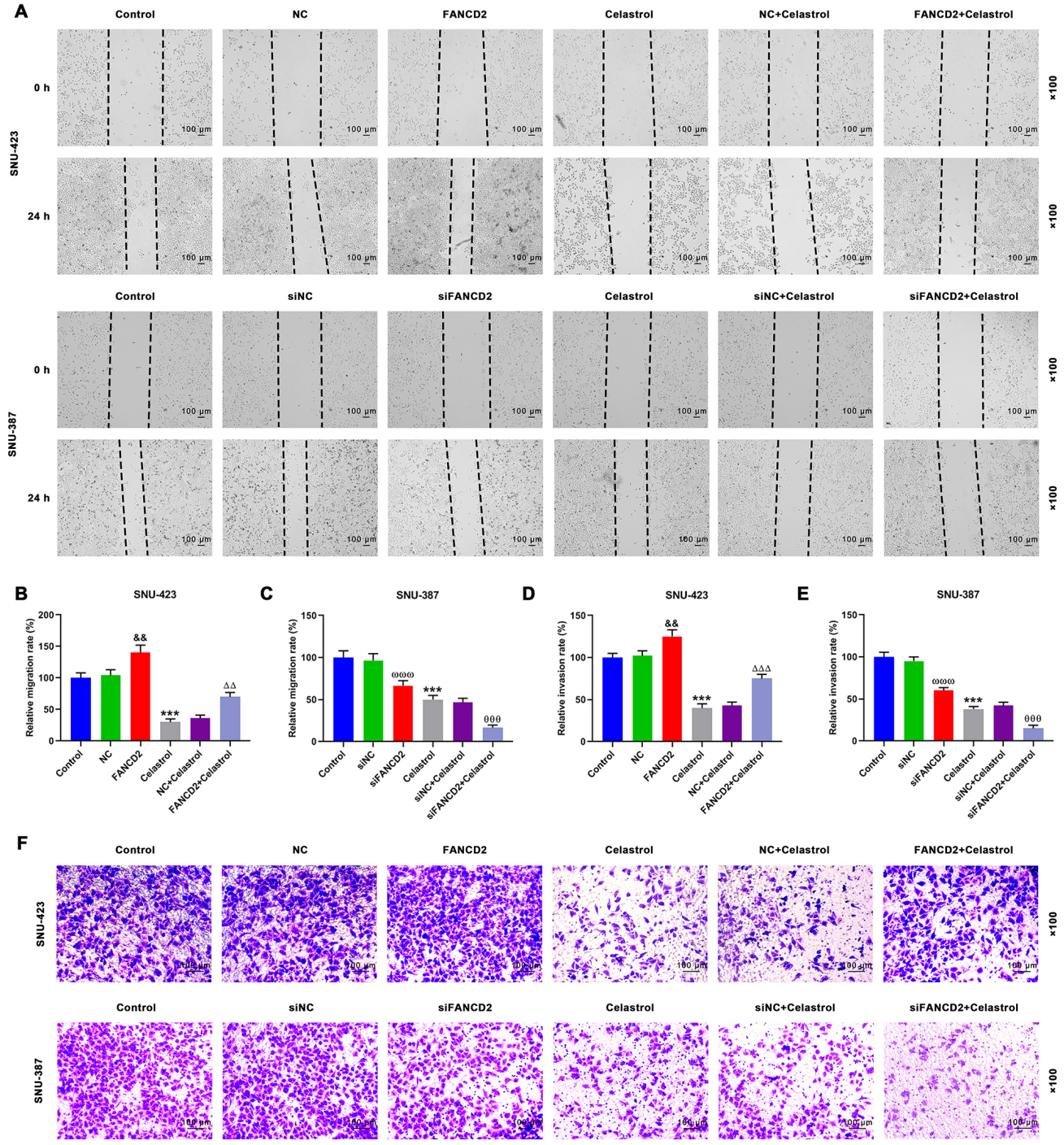

Fig. 8. Celastrol reversed the effects of overexpression *FANCD2* on HCC cell migration and invasion. (A–C) Migratory ability of SNU-423 cells after *FANCD2* plasmid/NC transfection and/or Celastrol (4 μM) treatment and that of SNU-387 cells after si*FANCD2*/siNC transfection and/or Celastrol (4 μM) treatment (cell scratch assay) (magnification: ×100; scale bar: 100 μm). (D–F) Invasive ability of SNU-423 cells after *FANCD2* plasmid/NC transfection and/or Celastrol treatment and that of SNU-387 cells after si*FANCD2*/siNC transfection and/or Celastrol treatment (Transwell invasion assay) (magnification: ×100; scale bar: 100 μm). $^{\&\&}p < 0.01$, vs. NC; $^{\omega\omega\omega}p < 0.001$, vs. siNC; ***$p < 0.001$, vs. Control; $^{\triangle\triangle}p < 0.01$, $^{\triangle\triangle\triangle}p < 0.001$, vs. NC+Celastrol; $^{\theta\theta\theta}p < 0.001$, vs. siNC+Celastrol. n = 3.

with *FANCD2*, a ferroptosis-inhibitory protein [30], and reduce expression of *FANCD2* in HCC cells. Based on these and the previously reported anti-HCC effects of Celastrol, we hypothesize that Celastrol targets *FANCD2* to promote ferroptosis in HCC cells, thereby suppressing HCC progression.

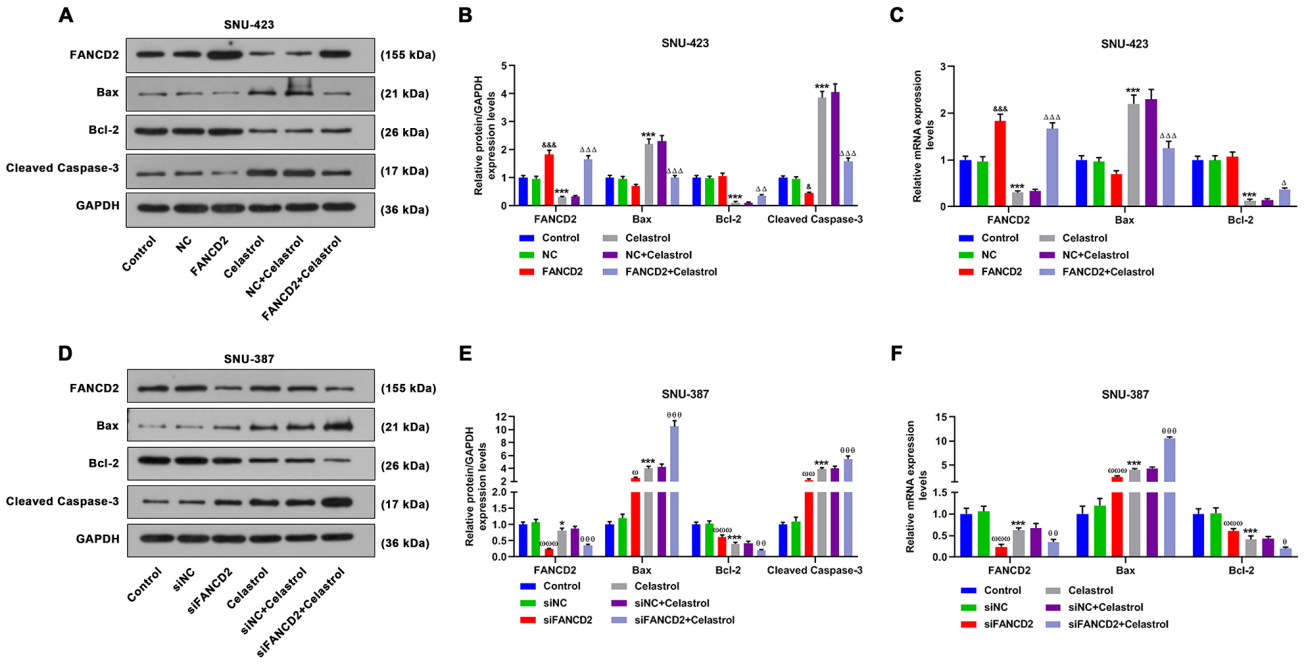

Fig. 9. Celastrol regulated the expressions of apoptosis-related factors in HCC cells by negatively regulating *FANCD2* expression. (A–F) FANCD2, Bax, Bcl-2, and cleaved caspase-3 expression in SNU-423 cells after *FANCD2* plasmid/NC transfection and/or Celastrol (4 μM) treatment and those in SNU-387 cells after si*FANCD2*/siNC transfection and/or Celastrol (4 μM) treatment (western blot (A,B,D,E) and/or qRT-PCR (C,F), GAPDH as an internal reference). $^{\&}p < 0.05$, $^{\&\&\&}p < 0.001$, vs. NC; $^{\omega}p < 0.05$, $^{\omega\omega}p < 0.01$, $^{\omega\omega\omega}p < 0.001$, vs. siNC; $^{*}p < 0.05$, $^{***}p < 0.001$, vs. Control; $^{\triangle}p < 0.05$, $^{\triangle\triangle}p < 0.01$, $^{\triangle\triangle\triangle}p < 0.001$, vs. NC+Celastrol; $^{\theta}p < 0.05$, $^{\theta\theta}p < 0.01$, $^{\theta\theta\theta}p < 0.001$, vs. siNC+Celastrol. n = 3.

FANCD2, a master regulator of the maintenance of common fragile sites in genomic regions [31], is an upregulated gene in HCC tissue specimens [32]. Moreover, high expression of *FANCD2* predicts poor prognoses in patients and is associated with larger tumor size; conversely, inhibition of *FANCD2* expression attenuates the proliferation of HCC cells [15], which signifies the growth-inhibitory role of *FANCD2* in HCC cells. Consistently, our study showed that high *FANCD2* expression in HCC cells was associated with the short survival time of patients, and *FANCD2* positively modulated HCC cell viability. The deficiency of *FANCD2* leads to DNA repair inhibition [33], which is accompanied by HCC cell apoptosis [34]. Bcl-2, Bax, and cleaved caspase-3, which are components of the apoptotic signaling pathway, play important roles in regulating apoptosis [35]. Bcl-2 is an antiapoptotic factor that inhibits cancer cell apoptosis and promotes survival, while Bax and cleaved caspase-3 promote apoptosis [36]. The present study revealed that HCC cell apoptosis, along with Bax and cleaved caspase-3 upregulation and Bcl-2 downregulation, was induced upon *FANCD2* knockdown. Celastrol can also induce HCC cell apoptosis [37]. In the present study, *FANCD2* knockdown and *FANCD2* overexpression were shown to potentiate or attenuate the pro-apoptotic effect of Celastrol in HCC cells, respectively, suggesting that targeting *FANCD2* can alter the growth-inhibitory effects of Celastrol in HCC.

Ferroptosis is often triggered with apoptosis to inhibit cell growth [38], and it is characterized by oxidative stress-induced membrane lipid peroxidation [39], which is triggered by ROS accumulation in the presence of excess iron [5]. MDA is produced as the principal byproduct of polyunsaturated fatty acid peroxidation [40]. SOD and GSH are both key antioxidant enzymes preventing oxidative stress [41]. In the present study, *FANCD2* overexpression increased SOD and GSH levels and decreased ROS levels, while *FANCD2* knockdown promoted MDA and ROS production and decreased SOD and GSH activity, suggesting that *FANCD2* protects HCC cells against oxidative stress. Although *FANCD2* inhibits ferroptosis [30], the level of iron in HCC cells was not affected by the manipulation of *FANCD2* expression. Furthermore, Celastrol significantly upregulated the level of iron in HCC cells, while Celastrol ameliorated oxidative stress in HCC cells, as previously reported [42]. These findings illustrate that Celastrol induced ferroptosis in HCC cells. We also discovered that *FANCD2* overexpression/knockdown weakened/strengthened the effect of Celastrol on ferroptosis in HCC cells, where Celastrol can downregulate *FANCD2*. Our results suggest that Celastrol reduced oxidative stress in HCC cells in part by decreasing *FANCD2* expression; however, whether *FANCD2* is involved in the ferroptosis-inhibitory effect of Celastrol in HCC cells remained unclear.

Autophagy, which is defined as a cellular degradation, promotes iron overload or directly induces lipid peroxidation to trigger ferroptosis when excessively activated [9]. Beclin, an ATG protein, forms protein complexes that are crucial to the formation of the autophagic vesicle membrane [43], after which autophagosome maturation is initiated [44] and LC3 is cleaved to generate LC3BI, which is then conjugated to the lipid phosphatidylethanolamine on the membrane, followed by the lipidation of LC3BI into LC3BII. Interestingly, the rate of lipidation reflects the extent of autophagosome formation [45]. Subsequently, autophagosomes, which engulf damaged organelles or misfolded proteins, are transported to the lysosome for degradation, completing the process of autophagy [46]. *FANCD2* is critical for autophagy-dependent ferroptosis [13], which is supported by the results of our study. We found that *FANCD2* negatively influenced autophagy in HCC cells, as its expression was negatively correlated with beclin and LC3BI/LC3BII. Given that excessive autophagy elicits ferroptosis, we inferred that *FANCD2* negatively regulates autophagy-ferroptosis in HCC cells. Meanwhile, Celastrol can enhance autophagy in HCC cells [47], consistent with our results. Taken together with our findings showing decreased *FANCD2* expression in HCC cells, these results indicate that Celastrol targets *FANCD2* to induce autophagy-dependent ferroptosis in HCC cells.

In addition, *FANCD2* is a key oncogene in HCC because HCC cell proliferation and invasion are dampened by *FANCD2* knockdown [15]. Inhibition of HepG2 cell migration is associated with *FANCD2* knockdown [48]. Consistent with these findings, our study demonstrated the migratory and invasive role of *FANCD2* in HCC cells. Furthermore, angiogenesis correlates with tumor cell migration and invasion, further leading to the onset of metastasis [49,50], a phenomenon responsible for the high recurrence and mortality rate of cancer [51]. Our study is the first to reveal that *FANCD2* has a positive correlation with *in vitro* angiogenesis prompted by HCC cells. Celastrol can suppress HCC progression by reducing tumor angiogenesis and inhibiting cancer cell growth, migration, and invasion [19,52]. In our study, the inhibitory effect of Celastrol on HCC cell angiogenesis, migration, and invasion was attenuated by *FANCD2* overexpression but was potentiated by *FANCD2* silencing, indicating that Celastrol suppressed *in vitro* HCC progression by downregulating *FANCD2*.

Conclusion

In conclusion, our study demonstrates that Celastrol promotes autophagy-dependent ferroptosis and inhibits angiogenesis, migration and invasion of HCC cells, and the anti-HCC effect of Celastrol may be the result of *FANCD2* inhibition.

Availability of Data and Materials

The analyzed data sets generated during the study are available from the corresponding author upon reasonable request.

Author Contributions

Substantial contributions to conception and design: JCY; data acquisition, data analysis and interpretation: TX; drafting the article or critically revising it for important intellectual content: JCY, TX; final approval of the version to be published: JCY, TX; agreement to be accountable for all aspects of the work in ensuring that questions related to the accuracy or integrity of the work are appropriately investigated and resolved: JCY, TX.

Ethics Approval and Consent to Participate

Not applicable.

Acknowledgment

Not applicable.

Funding

This research received no external funding.

Conflict of Interest

The authors declare no conflict of interest.

Supplementary Material

Supplementary material associated with this article can be found, in the online version, at https://doi.org/10.24976/Discov.Med.202537195.58.

References

[1] Boilève A, Hilmi M, Delaye M, Tijeras-Raballand A, Neuzillet C. Biomarkers in Hepatobiliary Cancers: What is Useful in Clinical Practice? Cancers. 2021; 13: 2708.

[2] Lian J, Zhang C, Lu H. A Ferroptosis-Related LncRNA Signature Associated with Prognosis, Tumor Immune Environment, and Genome Instability in Hepatocellular Carcinoma. Computational and Mathematical Methods in Medicine. 2022; 2022: 6284540.

[3] Wu Q, Hu Y, Ma Q, Yang S, Chen J, Wen S, *et al*. Comprehensive Analysis of RAPGEF2 for Predicting Prognosis and Immunotherapy Response in Patients with Hepatocellular Carcinoma. Journal of Oncology. 2022; 2022: 6560154.

[4] Ma Y, Sun WL, Ma SS, Zhao G, Liu Z, Lu Z, *et al*. LincRNA ZNF529-AS1 inhibits hepatocellular carcinoma via FBXO31 and predicts the prognosis of hepatocellular carcinoma patients. BMC Bioinformatics. 2023; 24: 54.

[5] Mou Y, Wang J, Wu J, He D, Zhang C, Duan C, *et al*. Ferroptosis, a new form of cell death: opportunities and challenges in cancer. Journal of Hematology & Oncology. 2019; 12: 34.

[6] Chen J, Li X, Ge C, Min J, Wang F. The multifaceted role of ferroptosis in liver disease. Cell Death and Differentiation. 2022; 29: 467–480.

[7] Zhu L, Lian W, Yao Z, Yang X, Wang Z, Lai Y, *et al*. Integrated Analysis of Ferroptosis and Immunity-Related Genes Associated with Intestinal Ischemia/Reperfusion Injury. Journal of Inflammation Research. 2022; 15: 2397–2411.

[8] Zhao T, Yu Z, Zhou L, Wang X, Hui Y, Mao L, *et al*. Regulating Nrf2-GPx4 axis by bicyclol can prevent ferroptosis in carbon tetrachloride-induced acute liver injury in mice. Cell Death Discovery. 2022; 8: 380.

[9] Liu J, Kuang F, Kroemer G, Klionsky DJ, Kang R, Tang D. Autophagy-Dependent Ferroptosis: Machinery and Regulation. Cell Chemical Biology. 2020; 27: 420–435.

[10] Li Y, Zhang H, Yang J, Zhan M, Hu X, Liu Y, *et al*. P2Y12 receptor as a new target for electroacupuncture relieving comorbidity of visceral pain and depression of inflammatory bowel disease. Chinese Medicine. 2021; 16: 139.

[11] Olazabal-Herrero A, He B, Kwon Y, Gupta AK, Dutta A, Huang Y, *et al*. The FANCI/FANCD2 complex links DNA damage response to R-loop regulation through SRSF1-mediated mRNA export. Cell Reports. 2024; 43: 113610.

[12] Ren JX, Li C, Yan XL, Qu Y, Yang Y, Guo ZN. Crosstalk between Oxidative Stress and Ferroptosis/Oxytosis in Ischemic Stroke: Possible Targets and Molecular Mechanisms. Oxidative Medicine and Cellular Longevity. 2021; 2021: 6643382.

[13] Miao H, Ren Q, Li H, Zeng M, Chen D, Xu C, *et al*. Comprehensive analysis of the autophagy-dependent ferroptosis-related gene FANCD2 in lung adenocarcinoma. BMC Cancer. 2022; 22: 225.

[14] Song L, Wu J, Fu H, Wu C, Tong X, Zhang M. Abnormally Expressed Ferroptosis-Associated FANCD2 in Mediating the Temozolomide Resistance and Immune Response in Glioblastoma. Frontiers in Pharmacology. 2022; 13: 921963.

[15] Komatsu H, Masuda T, Iguchi T, Nambara S, Sato K, Hu Q, *et al*. Clinical Significance of *FANCD2* Gene Expression and its Association with Tumor Progression in Hepatocellular Carcinoma. Anticancer Research. 2017; 37: 1083–1090.

[16] Wang Y, Wang Y. Analysis of the development course of traditional Chinese medicine standardization and recommendations on future work. Guidelines and Standards in Chinese Medicine. 2023; 1: 1–8.

[17] Zhang C, Wang W, Du C, Li H, Zhou K, Luan Z, *et al*. Autophagy in the pharmacological activities of celastrol (Review). Experimental and Therapeutic Medicine. 2023; 25: 268.

[18] Tao Z, Xiao Q, Che X, Zhang H, Geng N, Shao Q. Regulating mitochondrial homeostasis and inhibiting inflammatory responses through Celastrol. Annals of Translational Medicine. 2022; 10: 400.

[19] Si H, Wang H, Xiao H, Fang Y, Wu Z. Anti-Tumor Effect of Celastrol on Hepatocellular Carcinoma by the circ_SLIT3/miR-223-3p/CXCR4 Axis. Cancer Management and Research. 2021; 13: 1099–1111.

[20] Kun-Ming C, Chih-Hsien C, Chen-Fang L, Ting-Jung W, Hong-Shiue C, Wei-Chen L. Potential Anticancer Effect of Celastrol on Hepatocellular Carcinoma by Suppressing CXCR4-related Signal and Impeding Tumor Growth *in Vivo*. Archives of Medical Research. 2020; 51: 297–302.

[21] Du S, Song X, Li Y, Cao Y, Chu F, Durojaye OA, *et al*. Celastrol inhibits ezrin-mediated migration of hepatocellular carcinoma cells. Scientific Reports. 2020; 10: 11273.

[22] Zeng D, Zhang L, Luo Q. Celastrol-regulated gut microbiota and bile acid metabolism alleviate hepatocellular carcinoma proliferation by regulating the interaction between FXR and RXRα *in vivo* and *in vitro*. Frontiers in Pharmacology. 2023; 14: 1124240.

[23] Livak KJ, Schmittgen TD. Analysis of relative gene expression data using real-time quantitative PCR and the 2(-Delta Delta C(T)) Method. Methods. 2001; 25: 402–408.

[24] Hou M. Exploring novel independent prognostic biomarkers for hepatocellular carcinoma based on TCGA and GEO databases. Medicine. 2022; 101: e31376.

[25] Siegel RL, Miller KD, Jemal A. Cancer statistics, 2020. CA: A Cancer Journal for Clinicians. 2020; 70: 7–30.

[26] Yang J, Wei X, Hu F, Dong W, Sun L. Development and validation of a novel 3-gene prognostic model for pancreatic adenocarcinoma based on ferroptosis-related genes. Cancer Cell International. 2022; 22: 21.

[27] Ueda S, Nakamura H, Masutani H, Sasada T, Yonehara S, Takabayashi A, *et al*. Redox regulation of caspase-3(-like) protease activity: regulatory roles of thioredoxin and cytochrome c. Journal of Immunology. 1998; 161: 6689–6695.

[28] Hirschhorn T, Stockwell BR. The development of the concept of ferroptosis. Free Radical Biology & Medicine. 2019; 133: 130–143.

[29] Liu M, Fan Y, Li D, Han B, Meng Y, Chen F, *et al*. Ferroptosis inducer erastin sensitizes NSCLC cells to celastrol through activation of the ROS-mitochondrial fission-mitophagy axis. Molecular Oncology. 2021; 15: 2084–2105.

[30] Ren Z, Hu M, Wang Z, Ge J, Zhou X, Zhang G, *et al*. Ferroptosis-Related Genes in Lung Adenocarcinoma: Prognostic Signature and Immune, Drug Resistance, Mutation Analysis. Frontiers in Genetics. 2021; 12: 672904.

[31] Pladevall-Morera D, Munk S, Ingham A, Garribba L, Albers E, Liu Y, *et al*. Proteomic characterization of chromosomal common fragile site (CFS)-associated proteins uncovers ATRX as a regulator of CFS stability. Nucleic Acids Research. 2019; 47: 8004–8018.

[32] Tang X, Luo B, Huang S, Jiang J, Chen Y, Ren W, *et al*. FANCD2 as a novel prognostic biomarker correlated with immune and drug therapy in Hepatitis B-related hepatocellular carcinoma. European Journal of Medical Research. 2023; 28: 419.

[33] Nepal M, Che R, Ma C, Zhang J, Fei P. FANCD2 and DNA Damage. International Journal of Molecular Sciences. 2017; 18: 1804.

[34] Oda Y, Hidaka M, Suzuki A. Caffeine Has a Synergistic Anticancer Effect with Cisplatin via Inhibiting Fanconi Anemia Group D2 Protein Monoubiquitination in Hepatocellular Carcinoma Cells. Biological & Pharmaceutical Bulletin. 2017; 40: 2005–2009.

[35] Zhang Y, Yang X, Ge X, Zhang F. Puerarin attenuates neurological deficits via Bcl-2/Bax/cleaved caspase-3 and Sirt3/SOD2 apoptotic pathways in subarachnoid hemorrhage mice. Biomedicine & Pharmacotherapy. 2019; 109: 726–733.

[36] Kim IY, Kim HY, Song HW, Park JO, Choi YH, Choi E. Functional enhancement of exosomes derived from NK cells by IL-15 and IL-21 synergy against hepatocellular carcinoma cells: The cytotoxicity and apoptosis in vitro study. Heliyon. 2023; 9: e16962.

[37] Shen B, Chen HB, Zhou HG, Wu MH. Celastrol induces caspase-dependent apoptosis of hepatocellular carcinoma cells by suppression of mammalian target of rapamycin. Journal of Traditional Chinese Medicine. 2021; 41: 381–389.

[38] Wan P, Li T, Zhou L, Zhang J, Rao X. Eukaryotic Translation Initiation Factor 5A Independently Predicts Poor Prognosis of Cholangiocarcinoma Patients and Regulates the Ferroptosis and Mitochondrial Apoptosis. Journal of Oncology. 2022; 2022: 4250531.

[39] Taylor WR, Fedorka SR, Gad I, Shah R, Alqahtani HD, Koranne R, *et al*. Small-Molecule Ferroptotic Agents with Potential to Selectively Target Cancer Stem Cells. Scientific Reports. 2019; 9: 5926.

[40] Morales M, Munné-Bosch S. Malondialdehyde: Facts and Arti-

facts. Plant Physiology. 2019; 180: 1246–1250.
[41] Ali SS, Ahsan H, Zia MK, Siddiqui T, Khan FH. Understanding oxidants and antioxidants: Classical team with new players. Journal of Food Biochemistry. 2020; 44: e13145.
[42] Jannuzzi AT, Kara M, Alpertunga B. Celastrol ameliorates acetaminophen-induced oxidative stress and cytotoxicity in HepG2 cells. Human & Experimental Toxicology. 2018; 37: 742–751.
[43] Kang R, Zeh HJ, Lotze MT, Tang D. The Beclin 1 network regulates autophagy and apoptosis. Cell Death and Differentiation. 2011; 18: 571–580.
[44] Wilson MI, Dooley HC, Tooze SA. WIPI2b and Atg16L1: setting the stage for autophagosome formation. Biochemical Society Transactions. 2014; 42: 1327–1334.
[45] Onorati AV, Dyczynski M, Ojha R, Amaravadi RK. Targeting autophagy in cancer. Cancer. 2018; 124: 3307–3318.
[46] Yang Z, Klionsky DJ. Mammalian autophagy: core molecular machinery and signaling regulation. Current Opinion in Cell Biology. 2010; 22: 124–131.
[47] Ren B, Liu H, Gao H, Liu S, Zhang Z, Fribley AM, *et al*. Celastrol induces apoptosis in hepatocellular carcinoma cells via targeting ER-stress/UPR. Oncotarget. 2017; 8: 93039–93050.
[48] Kui XY, Gao Y, Liu XS, Zeng J, Yang JW, Zhou LM, *et al*. Comprehensive Analysis of SLC17A9 and Its Prognostic Value in Hepatocellular Carcinoma. Frontiers in Oncology. 2022; 12: 809847.
[49] Sobocińska AA, Czarnecka AM, Szczylik C. Mechanisms of angiogenesis in neoplasia. Postepy Higieny i Medycyny Doswiadczalnej (Online). 2016; 70: 1166–1181.
[50] Viallard C, Larrivée B. Tumor angiogenesis and vascular normalization: alternative therapeutic targets. Angiogenesis. 2017; 20: 409–426.
[51] Duff D, Long A. Roles for RACK1 in cancer cell migration and invasion. Cellular Signalling. 2017; 35: 250–255.
[52] Rajendran P, Li F, Shanmugam MK, Kannaiyan R, Goh JN, Wong KF, *et al*. Celastrol suppresses growth and induces apoptosis of human hepatocellular carcinoma through the modulation of STAT3/JAK2 signaling cascade *in vitro* and *in vivo*. Cancer Prevention Research. 2012; 5: 631–643.